JAAS

TECHNICAL NOTE

View Article Online
View Journal | View Issue

Cite this: J. Anal. At. Spectrom., 2016, 31, 809

Temporal changes of size distribution of mass and relative intensity for ablated particles during laser ablation inductively coupled plasma mass spectrometry

Ryo Machida, Takashi Nakazawa and Naoki Furuta*

To investigate elemental fractionation during laser ablation-inductively coupled plasma mass spectrometry (LA-ICPMS) we measured mass fractions of ablated particles and chemical composition of ablated particles in this study. Temporal changes of fractionation indexes (FIs) were investigated under laser defocus conditions which caused a large variation of size distribution of abated particles. It was a useful technique for understanding the relationship between temporal changes of FIs and the size of ablated particles. Ablated particles were fractionated by aerodynamic diameters (<0.06, 0.06–0.22, 0.22–2.2, and >2.2 μm) with a low-pressure impactor and were digested with HNO_3 and HF; then As, Rb, Rh, La, Gd, Yb, W, Re, and Th were measured by ICPMS. Under 0.5 mm defocus and 1.0 mm defocus conditions, the mass fractions (ablated particle mass at 1–5 min divided by that at 0–1 min) of ablated particles larger than 0.22 μm were larger than the mass fractions of ablated particles smaller than 0.22 μm. Volatile elements such as As and Rb were enriched in particles smaller than 0.22 μm, owing to the large aspect ratio of the crater under defocus conditions. However, the magnitude of the enrichment for volatile elements did not change as ablation progressed. Therefore, we concluded that large particles could not be decomposed completely in the ICP and the FI peak observed at 2–3 min was caused by changes in elemental behavior due to changes in ablated particles larger than 0.22 μm.

Received 24th October 2015
Accepted 15th December 2015

DOI: 10.1039/c5ja00424a

www.rsc.org/jaas

1. Introduction

Laser ablation-inductively coupled plasma mass spectrometry (LA-ICPMS) is an effective technique for multielemental analysis of solid samples. However, LA-ICPMS suffers from elemental fractionation, whereby elements in a sample are enriched (or depleted) during the laser ablation process and in the plasma, to an extent that depends on the elemental properties.[1–4] The fractionation mechanism has not been definitively elucidated.[5–8] Elemental fractionation can be quantified in terms of the fractionation index (FI).[9–11] Temporal changes of FIs were investigated under laser defocus conditions. When laser ablation was performed under defocus conditions, a large variation of the diameter of ablated particles was observed. It was a useful technique for understanding the relationship between temporal changes of FIs and the size of ablated particles. We previously reported that temporal changes in FIs were caused by changes in elemental behavior resulting from changes in ablated particles with aerodynamic diameters (D_p) larger than 2.0 μm introduced into the ICP, which could not be decomposed completely in the ICP.[1] However, the variation of FIs for smaller ablated particles and the chemical composition of fine particles have not been sufficiently investigated. Koch *et al.* studied the particle size distributions and composition of a brass sample.[12] In the current study, we used a NIST 610 glass standard material as a sample. Four fractions of size-classified ablated particles (D_p values of <0.06, 0.06–0.22, 0.22–2.2, and >2.2 μm) were collected on filters and digested with HNO_3 and HF, and then the elements in the particles were determined by ICPMS. Elemental fractionation is discussed on the basis of the size distribution of mass and the relative intensity of metal and ytterbium.

2. Experimental

2.1 Instrumentation

A laser ablation system (UP-213, ESI, Portland, OR, USA) combined with an ICPMS instrument (Agilent 7500ce, Agilent Technologies, Tokyo, Japan) was used to analyze a NIST 610 (National Institute of Standards and Technology, Maryland, USA) glass standard sample. The beam of the laser system was a flat top shape under in focus conditions. A commercially available large-format (15 sq. cm) laser ablation cell (ESI, Portland, OR, USA) was used. To reduce wash-out time,

Faculty of Science and Engineering, Department of Applied Chemistry, Chuo University, 1-13-27 Kasuga, Bunkyo-ku, Tokyo 112-8551, Japan. E-mail: nfuruta@chem.chuo-u.ac.jp; Fax: +81-3-3817-1906; Tel: +81-3-3817-1906

a quartz ring with a volume of approximately 0.8 cm^3 was put inside the large-format cell. Laser ablation was carried out in a He atmosphere, and the ablated particles were introduced into a cascade impactor (inline type with NL-1-1A (<1.0 μm), Tokyo Dylec, Tokyo, Japan), which removes ablated particles larger than 1.0 μm. Ar gas was introduced between the large-format cell and the cascade impactor. The LA-ICPMS measurement conditions used in this study are summarized in Table 1. In focus, 0.5 mm defocus, and 1.0 mm defocus conditions were used to evaluate the effects of defocus conditions. These three focus conditions were selected as typical trends of temporal changes of FIs. Under −1.0 mm defocus and 1.5 mm defocus conditions, no signal was observed by LA-ICPMS. Temporal changes of FIs under −0.5 mm defocus conditions showed the same trend as those under in focus conditions.

Table 1 Operating conditions used for laser ablation and ICPMS measurements

Laser ablation	
Laser model	UP213
Laser type	Nd:YAG
Wavelength	213 nm
Pulse width	4 ns
Ablation mode	Single site
Repetition rate	20 Hz
Carrier gas (He) flow rate	1.0 L min^{-1}
Laser energy on the sample surface	0.9 mJ
Initial laser fluence[a]	
In focus	11 J cm^{-2}
0.5 mm defocus	30 J cm^{-2}
1.0 mm defocus	3.0 J cm^{-2}
Crater diameter	
In focus	100 ± 5 μm
0.5 mm defocus	60 ± 4 μm
1.0 mm defocus	200 ± 10 μm
Crater depth	
In focus	380 ± 30 μm
0.5 mm defocus	1500 ± 150 μm
1.0 mm defocus	1600 ± 150 μm

ICPMS measurements		
ICPMS model		Agilent 7500cc
RF power		1600 W
Integration time		0.05 s
Collision gas (He) flow rate		2.0 mL min^{-1}
	for laser ablation	for solution nebulization
Carrier gas (Ar) flow rate	0.8 L min^{-1}	1.2 L min^{-1}
Sample uptake rate	—	0.1 mL min^{-1}
Isotopes measured	^{42}Ca, ^{75}As	^{75}As, ^{85}Rb, ^{103}Rh, ^{139}La, ^{157}Gd, ^{173}Yb, ^{182}W, ^{185}Re, ^{232}Th

[a] Actual fluence changed with time.

An optical microscope (VHX-2000, Keyence, Osaka, Japan) was used for detailed observation of the crater. Crater diameters and depths were measured by observing the sample from the top and from the side, respectively, after laser irradiation under in focus, 0.5 mm defocus, and 1.0 mm defocus conditions. When laser ablation was performed for 10 min, 12 000 shots (20 Hz × 600 s) of laser pulses were irradiated on the sample surface. The crater diameters were 100, 60, and 200 μm, respectively, and the crater depths were 380, 1500, and 1600 μm, respectively. The craters were a top hat shape under in focus conditions and a reverse circular cone shape under defocus conditions.

2.2 Reagents

HF (25 M, Daikin Industries, Osaka, Japan) and HNO_3 (ultrapure, 11 M, Kanto Chemical, Tokyo, Japan) were used for acid digestion. Calibration standard solutions were prepared from the following SPEX CertiPrep (Metuchen, NJ, USA) multielement standards for ICPMS: XSTC-1, XSTC-8, and XSTC-13. The standards were diluted with 0.1 M HNO_3. Calibration curves were prepared by the measurement of standard solutions at concentrations of 0, 10, 100, 500, and 5000 pg mL^{-1}.

2.3 Collection of size-classified ablated particles with a low-pressure impactor

Four fractions of size-classified ablated particles (D_p values of <0.06, 0.06–0.22, 0.22–2.2, and >2.2 μm) were collected by means of a low-pressure impactor (LP-20; Tokyo Dylec Co., Tokyo, Japan), which was placed in an ISO class 4 clean bench equipped with HEPA filters (Fig. 1). Particle fractions were collected on PTFE filters (T010A080C, 80 mm diameter, Advantec Toyo Kaisha, Tokyo, Japan), except for the finest fraction (<0.06 μm), which was collected on a quartz fiber filter (2500 QAT-UP; 80 mm diam., Pall Corporation, Port Washington, NY, USA).

2.4 Acid digestion

The collected particles were decomposed with a mixture of 25 M HF (0.3 mL) and 11 M HNO_3 (0.6 mL) at 180 °C on a hotplate. Heating continued until the HF had evaporated completely and the digested solution became one droplet. Then, the digested solution was diluted to 2 mL with 0.1 M HNO_3. As an internal standard, 20 ng of Rh was added into the samples.

3. Results and discussion

3.1 Fractionation index obtained by means of LA-ICPMS with a cascade impactor

Using the single-site mode under in focus, 0.5 mm defocus, and 1.0 mm defocus conditions, we measured the elemental intensities of As and Ca by means of time-resolved analysis. In the previous paper,[1] 34 elements were classified into two groups in accordance with their observed temporal changes of FIs. Elements in the first group (Group 1) showed the FI peak at 2–3 min after the start of laser ablation under defocus conditions. Volatile elements such as As are included in the first group.

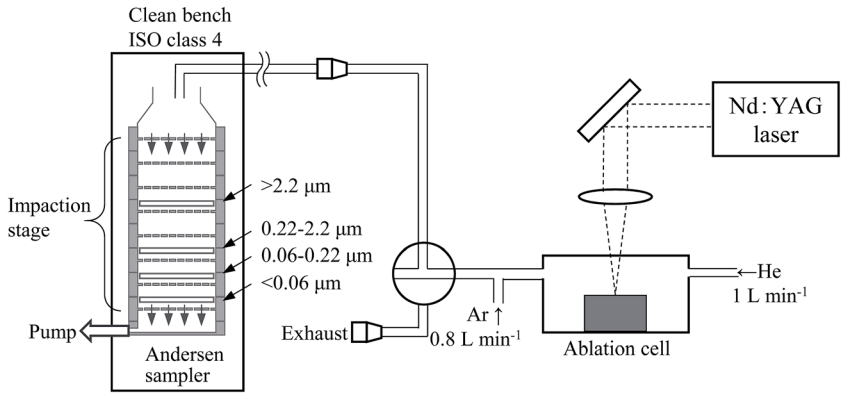

Fig. 1 Schematic diagram of the experimental setup used to collect ablated particles on four separate filters.

Elements in the second group (Group 2) did not show the FI peak as laser ablation progressed. Non-volatile elements such as Ca are included in the second group. For this set of experiments, As was selected as a typical element of the first group of elements. The signal intensities and FIs for As as a function of ablation time are shown in Fig. 2.

Under the in focus conditions, the plot of FIs for As did not show a peak at an ablation time of 2–3 min, whereas a peak in FIs was observed at 2–3 min under the 0.5 mm defocus and 1.0 mm defocus conditions (Fig. 2d–f). The magnitudes of the FI peaks were 2.3 without the 1.0 μm impactor and 1.9 with the impactor under the 0.5 mm defocus conditions. Under the 1.0 mm defocus conditions, the corresponding magnitudes were 1.9 and 1.4, respectively. That is, although the FI peak was suppressed by the use of the impactor, the peak did not disappear completely.

3.2 Mass of size-classified ablated particles collected with a low-pressure impactor

The size-classified ablated particles were collected on different filters by means of a low-pressure impactor sampler. The particle fractions were decomposed with acid, and ICPMS was

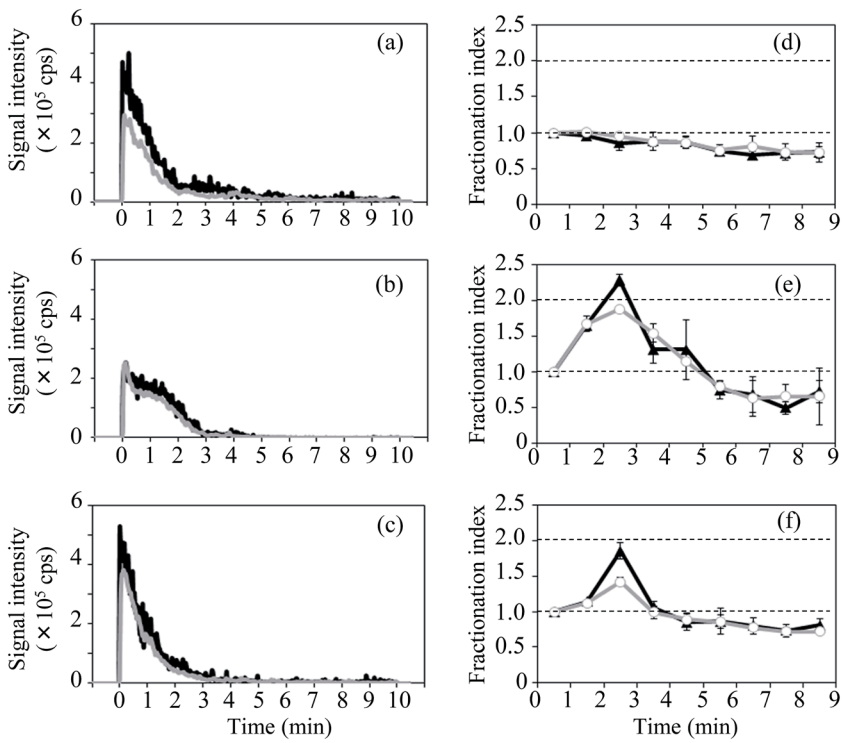

Fig. 2 Signal intensities of As obtained by LA-ICPMS. Laser ablation was performed under (a) in-focus, (b) 0.5 mm defocus, and (c) 1.0 mm defocus conditions without (black) and with (gray) a 1.0 μm impactor. Fractionation indexes of As during laser ablation under (d) in-focus, (e) 0.5 mm defocus, and (f) 1.0 mm defocus conditions without (triangles) and with (circles) a 1.0 μm impactor. Error bars indicate standard deviations ($n = 3$).

used to determine Yb, which was suitable for estimation of the mass of ablated particles because the background was low and the sensitivity was high for ICPMS measurements. Moreover, Yb is typical for the elements classified as Group 2 in our previous study.[1] The mass of ablated particles was calculated from the mass of Yb by dividing by the certified value for Yb (473 μg g^{-1}) in the NIST 610 glass standard. A mass fraction was calculated by dividing the mass of ablated particles at 1–5 min by the mass of ablated particles at 0–1 min.

The masses of ablated particles and the mass fractions of the size-classified ablated particles are shown in Fig. 3. The total masses of ablated particles collected at 0–1 min of ablation under in focus, 0.5 mm defocus, and 1.0 mm defocus conditions were 15.2, 10.2, and 8.8 pg, respectively, and the total masses of ablated particles collected at 1–5 min under in focus, 0.5 mm defocus, and 1.0 mm defocus conditions were 5.1, 3.6, and 3.2 pg, respectively. The ratios of the total masses collected at 1–5 min to the total masses collected at 0–1 min of ablation were 34%, 35%, and 36% under in focus, 0.5 mm defocus, and 1.0 mm defocus conditions, respectively. Under the defocus conditions, the mass fractions of particles larger than 0.22 μm were high: specifically, 57% (0.22–2.2 μm) and 59% (>2.2 μm) under the 0.5 mm defocus conditions and 54% (0.22–2.2 μm) and 51% (>2.2 μm) under the 1.0 mm defocus conditions. These results confirm that the mass of particles larger than 0.22 μm was higher at 1–5 min than at 0–1 min when laser ablation was performed under defocus conditions.

Smaller particles (<0.06 μm) were produced in greater amounts than larger particles. However, under all three focus conditions, the mass fractions of these smaller particles were the same as the ratios of the total masses collected at 1–5 min to the total masses collected at 0–1 min of ablation. The mass fractions of the larger particles increased under defocus conditions. Therefore, we concluded that the FI peak at 2–3 min was caused by changes in ablated particles larger than 0.22 μm.

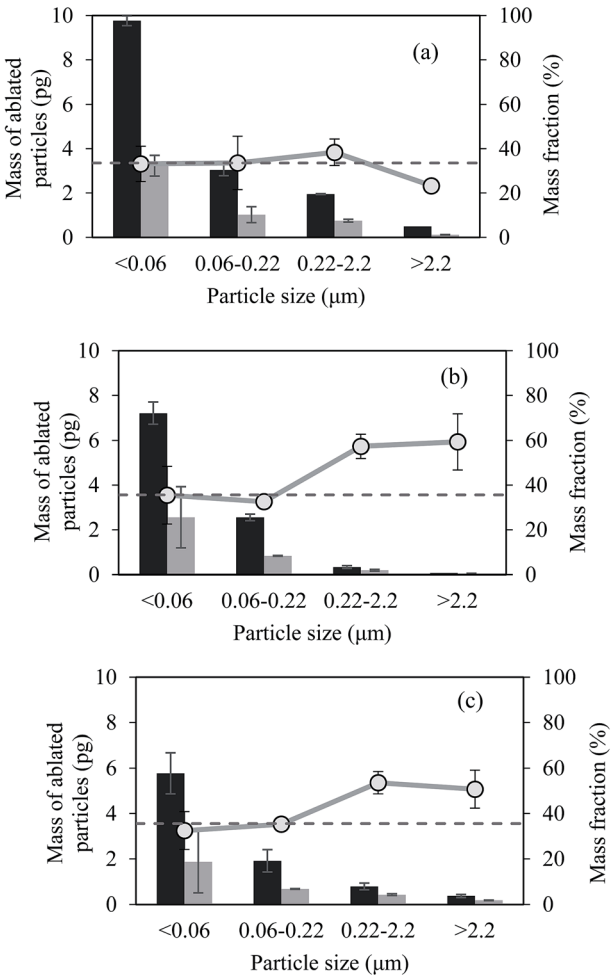

Fig. 3 Masses of ablated particles (bars) and mass fractions of size-classified ablated particles (gray circles) obtained under (a) in focus, (b) 0.5 mm defocus, and (c) 1.0 mm defocus conditions at 0–1 min of ablation (black bars) and at 1–5 min of ablation (gray bars). Dashed lines indicate the ratios of the total masses collected at 1–5 min to the total masses collected at 0–1 min. Error bars indicate standard deviations (n = 3).

3.3 Chemical composition of size-classified ablated particles

The amounts of As, Rb, Re, W, La, Gd, Th, and Yb in the size-classified ablated particles were determined by means of ICPMS, and temporal FIs were calculated from eqn (1):

$$\text{Temporal FI} = \left[\frac{(\text{M/Yb})_{1-5\ \text{min}}}{(\text{M/Yb})_{0-1\ \text{min}}}\right] \quad (1)$$

where $(\text{M/Yb})_{1-5\ \text{min}}$ is the relative intensity of element M normalized by the signal intensity of Yb at 1–5 min of ablation, and $(\text{M/Yb})_{0-1\ \text{min}}$ is the relative intensity of element M normalized by the signal intensity of Yb at 0–1 min of ablation. The relative intensities and temporal FIs of all the elements, along with the melting points (mp) of their oxides, are listed in Table 2. The temporal FIs of the first group of elements (Group 1) were between 0.8 and 1.2 and those of the second group of elements (Group 2) were between 0.9 and 1.1. All the FIs were approximately 1 and did not depend on the size of the ablated particles, indicating that the magnitude of the enrichment did not change as laser ablation progressed.

The crater aspect ratios under in focus (11 J cm^{-2}), 0.5 mm defocus (30 J cm^{-2}), and 1.0 mm defocus (3.0 J cm^{-2}) conditions were 3.8, 25, and 8.0, respectively. The fluence was calculated from the diameter of the crater produced on the sample surface. The actual fluence increased as laser ablation progressed. For the elemental composition, the relative intensities of As in the particles smaller than 0.06 μm at 0–1 min of ablation under in focus, 0.5 mm defocus, and 1.0 mm defocus conditions were 0.08, 0.20, and 0.13, respectively. The corresponding values for Rb were 1.53, 2.73, and 1.81. The relative intensities of the volatile elements under 0.5 mm defocus conditions were larger than those of the ones under in focus and 1.0 mm defocus conditions. However, the relative intensities of the elements in Group 2 were constant regardless of the focus conditions. The relative intensities of volatile elements increased as the aspect ratio of the crater increased. The relative intensities of As at 0–1 min of ablation under 0.5 mm defocus conditions were 0.20, 0.17, 0.09, and 0.11 for particles with sizes of <0.06, 0.06–0.22,

Table 2 Relative intensity data of size-classified particles and temporal FIs of elements along with melting points of their oxides

			<0.06 μm			0.06–0.22 μm			0.22–2.2 μm			>2.2 μm		
Group[a]	Element	Mp of oxide (°C)	Relative intensity $(M/Yb)_{0-1}$	$(M/Yb)_{1-5}$	Temporal FI	Relative intensity $(M/Yb)_{0-1}$	$(M/Yb)_{1-5}$	Temporal FI	Relative intensity $(M/Yb)_{0-1}$	$(M/Yb)_{1-5}$	Temporal FI	Relative intensity $(M/Yb)_{0-1}$	$(M/Yb)_{1-5}$	Temporal FI
Aerodynamic diameter under in focus conditions														
1	As	274	0.08	0.09	1.1 ± 0.2	0.04	0.05	1.1 ± 0.2	0.04	0.05	1.1 ± 0.2	0.06	0.05	1.0 ± 0.2
1	Rb	412	1.53	1.66	1.1 ± 0.0	0.84	0.94	1.1 ± 0.1	0.87	0.77	0.9 ± 0.1	0.99	0.96	1.0 ± 0.2
1	Re	900	0.19	0.17	0.9 ± 0.1	0.15	0.17	1.1 ± 0.1	0.15	0.15	1.0 ± 0.2	0.18	0.16	0.9 ± 0.2
1	W	1500	1.01	0.90	0.9 ± 0.1	0.88	0.92	1.0 ± 0.1	0.94	0.76	0.8 ± 0.2	0.90	0.85	0.9 ± 0.0
2	La	2315	3.47	3.51	1.0 ± 0.1	3.34	3.53	1.1 ± 0.1	3.45	3.37	1.0 ± 0.0	3.79	3.36	0.9 ± 0.1
2	Gd	2339	0.75	0.76	1.0 ± 0.2	0.72	0.77	1.1 ± 0.1	0.72	0.73	1.0 ± 0.0	0.82	0.80	1.0 ± 0.4
2	Th	3390	3.00	2.64	0.9 ± 0.1	3.41	3.48	1.0 ± 0.0	3.45	3.47	1.0 ± 0.0	3.39	3.38	1.0 ± 0.0
Aerodynamic diameter under 0.5 mm defocus conditions														
1	As	274	0.20	0.22	1.1 ± 0.1	0.17	0.20	1.2 ± 0.2	0.09	0.09	1.0 ± 0.3	0.11	0.10	0.9 ± 0.2
1	Rb	412	2.73	2.60	1.0 ± 0.3	1.68	1.70	1.0 ± 0.2	0.91	0.80	0.9 ± 0.1	0.96	0.95	1.0 ± 0.2
1	Re	900	0.16	0.16	1.0 ± 0.2	0.36	0.37	1.0 ± 0.2	0.17	0.15	0.9 ± 0.2	0.11	0.10	0.9 ± 0.3
1	W	1500	1.47	1.47	1.0 ± 0.1	1.97	2.15	1.1 ± 0.2	1.14	1.03	0.9 ± 0.1	1.14	1.12	1.0 ± 0.3
2	La	2315	3.73	3.42	0.9 ± 0.1	3.90	3.73	1.0 ± 0.1	3.37	3.43	1.0 ± 0.1	2.89	3.02	1.0 ± 0.1
2	Gd	2339	0.84	0.88	1.1 ± 0.1	0.79	0.75	0.9 ± 0.1	0.68	0.63	0.9 ± 0.1	0.77	0.77	1.0 ± 0.3
2	Th	3390	2.73	2.88	1.1 ± 0.1	3.01	3.01	1.0 ± 0.0	2.85	2.75	1.0 ± 0.1	2.65	2.81	1.1 ± 0.3
Aerodynamic diameter under 1.0 mm defocus conditions														
1	As	274	0.13	0.15	1.1 ± 0.3	0.06	0.05	0.9 ± 0.1	0.06	0.05	1.0 ± 0.2	0.09	0.10	1.1 ± 0.1
1	Rb	412	1.81	1.68	0.9 ± 0.2	0.84	0.92	1.1 ± 0.2	0.84	0.81	1.0 ± 0.1	0.91	0.92	1.0 ± 0.3
1	Re	900	0.19	0.18	1.0 ± 0.2	0.16	0.17	1.1 ± 0.1	0.12	0.12	1.0 ± 0.2	0.17	0.18	1.0 ± 0.3
1	W	1500	1.04	1.15	1.1 ± 0.4	N. D.	N. D.	—	N. D.	N. D.	—	N. D.	N. D.	—
2	La	2315	3.14	3.46	1.1 ± 0.1	3.52	3.85	1.1 ± 0.1	3.51	3.69	1.1 ± 0.1	3.63	3.98	1.1 ± 0.2
2	Gd	2339	0.67	0.76	1.1 ± 0.3	0.74	0.78	1.1 ± 0.1	0.75	0.71	0.9 ± 0.1	0.77	0.81	1.1 ± 0.2
2	Th	3390	3.20	2.96	0.9 ± 0.3	3.36	3.40	1.0 ± 0.0	3.34	3.11	0.9 ± 0.1	3.27	3.62	1.1 ± 0.2

[a] Ref. 1.

0.22–2.2, and >2.2 μm, respectively. The relative intensities of As in particles smaller than 0.22 μm were larger than those of As in particles larger than 0.22 μm. The same trend was observed for Rb. We confirmed that during laser ablation, the magnitude of the enrichment varied with the aspect ratio.[13] Volatile elements were enriched in smaller particles because smaller particles were generated by hydrodynamic sputtering in the heat-effective zone on the sample surface. The size dependence of the chemical composition of the particles was caused by noncongruent evaporation.[14–16]

However, the relative intensities of elements in Group 1 at 1–5 min of ablation were the same as those observed at 0–1 min of ablation. That is, the magnitude of the enrichment of the elements in Group 1 at 0–1 min of ablation was the same as that at 1–5 min of ablation. This result indicates that the FI peak observed for elements in Group 1 at 2–3 min after the start of laser ablation was not caused by smaller particles but by particles larger than 0.22 μm. Particles larger than 0.22 μm could not be decomposed completely in the ICP and elements in Group 1 were more easily vaporized and ionized than Ca.

4. Conclusions

In this study, ablated particles were classified by the size, and the chemical composition of the particles was investigated. The FI peak observed for elements in Group 1 under defocus conditions at 2–3 min after the start of laser ablation was suppressed by the use of a 1.0 μm impactor, but the peak did not disappear completely. Under the in focus conditions, the mass fraction of ablated particles did not change. In contrast, under 0.5 mm defocus and 1.0 mm defocus conditions, the mass fraction of ablated particles increased for ablated particles larger than 0.22 μm.

Volatile elements were enriched in small particles produced during laser ablation regardless of the focus conditions. The magnitude of the enrichment increased as the aspect ratio of the crater increased. However, the magnitude of the enrichment at 0–1 min of ablation was the same as that at 1–5 min of ablation. These experimental results indicate that the FI peak observed for Group 1 elements under defocus conditions at 2–3 min after the start of ablation was not caused by smaller particles but by particles larger than 0.22 μm. Particles larger than 0.22 μm could not be decomposed completely in the ICP and elements in Group 1 were more easily vaporized and ionized than Ca.

Acknowledgements

This research was supported by the Ministry of Education, Culture, Sports, Science and Technology, Japan, through a Grant-in-Aid for Scientific Research (C) (no. 26410160) and a Grant-in-Aid for Young Scientists (B) (no. 26870595). Part of this study was supported under a joint research project conducted at the Institute of Science and Engineering of Chuo University.

References

1 R. Machida, T. Nakazawa and N. Furuta, *Anal. Sci.*, 2015, **31**, 345–355.
2 R. E. Russo, X. Mao, J. J. Gonzalez, V. Zorba and J. Yoo, *Anal. Chem.*, 2013, **85**, 6162–6177.
3 R. E. Russo, X. Mao, H. Liu, J. Gonzalez and S. S. Mao, *Talanta*, 2002, **57**, 425–451.
4 H. P. Longerich, D. Günther and S. E. Jackson, *Fresenius. J. Anal. Chem.*, 1996, **355**, 538–542.
5 D. Günther and C. A. Heinrich, *J. Anal. At. Spectrom.*, 1999, **14**, 1369–1374.
6 Z. Wang, B. Hattendorf and D. Günther, *J. Am. Soc. Mass Spectrom.*, 2006, **17**, 641–651.
7 C. Liu, X. L. Mao, S. S. Mao, X. Zeng, R. Greif and R. E. Russo, *Anal. Chem.*, 2004, **76**, 379–383.
8 T. Hirata and Y. Kon, *Anal. Sci.*, 2008, **24**, 345–353.
9 I. Kroslakova and D. Günther, *J. Anal. At. Spectrom.*, 2007, **22**, 51–62.
10 T. E. Jeffries, S. E. Jackson and H. P. Longerich, *J. Anal. At. Spectrom.*, 1998, **13**, 935–940.
11 M. Ohata, D. Tabersky, R. Glaus, J. Koch, B. Hattendorf and D. Günther, *J. Anal. At. Spectrom.*, 2014, **29**, 1345–1353.
12 J. Koch, A. von Bohlen, R. Hergenröder and K. Niemax, *J. Anal. At. Spectrom.*, 2004, **19**, 267–272.
13 O. V. Borisov, X. Mao and R. E. Russo, *Spectrochim. Acta, Part B*, 2000, **55**, 1693–1704.
14 R. Hergenröder, *J. Anal. At. Spectrom.*, 2006, **21**, 505–516.
15 H. R. Kuhn and D. Günther, *J. Anal. At. Spectrom.*, 2004, **19**, 1158–1164.
16 R. Machida, T. Nakazawa, Y. Sakuraba, M. Fujiwara and N. Furuta, *J. Anal. At. Spectrom.*, 2015, **30**, 2412–2419.

